

Interorbital interaction in the one-dimensional periodic Anderson model: A density-matrix renormalization-group study

I. Hagymási^{1,2}, J. Sólyom¹, and Ö. Legeza¹

¹*Strongly Correlated Systems "Lendület" Research Group, Institute for Solid State Physics and Optics, MTA Wigner Research Centre for Physics, Budapest H-1525 P.O. Box 49, Hungary*

²*Department of Theoretical Physics, University of Szeged, Tisza Lajos krt 84-86, H-6720 Szeged, Hungary*
(Dated: June 19, 2021)

We investigate the effect of the Coulomb interaction, U_{cf} , between the conduction and f electrons in the periodic Anderson model using the density-matrix renormalization-group algorithm. We calculate the excitation spectrum of the half-filled symmetric model with an emphasis on the spin and charge excitations. In the one-dimensional version of the model it is found that the spin gap is smaller than the charge gap below a certain value of U_{cf} and the reversed inequality is valid for stronger U_{cf} . This behavior is also verified by the behavior of the spin and density correlation functions. We also perform a quantum information analysis of the model and determine the entanglement map of the f and conduction electrons. It is revealed that for a certain U_{cf} the ground state is dominated by the configuration in which the conduction and f electrons are strongly entangled, and the ground state is almost a product state. For larger U_{cf} the sites are occupied alternately dominantly by two f electrons or by two conduction electrons.

PACS numbers: 71.10.Fd, 71.27.+a, 75.30.Mb

I. INTRODUCTION

Kondo insulators are a peculiar group of rare-earth materials, which behave as metals with magnetic moments above a characteristic temperature (~ 100 K) and become semiconductors at low temperatures due to strong correlations.¹ Gaps are opened in both the spin and charge sectors, and they are in the order of a few meV, which defines the small energy scale of these compounds. These small gaps cannot be understood in a simple band picture, since the strong interaction between the electrons plays a crucial role. Furthermore this is the reason why different energy scales arise in the spin and charge sectors.

The minimal model for the Kondo insulators is the half-filled periodic Anderson model² (PAM). In its one-dimensional version the Hamiltonian reads

$$\begin{aligned} \mathcal{H}_{\text{PAM}} = & -t \sum_{j,\sigma} (\hat{c}_{j\sigma}^\dagger \hat{c}_{j+1\sigma} + \hat{c}_{j+1\sigma}^\dagger \hat{c}_{j\sigma}) \\ & - V \sum_{j,\sigma} (\hat{f}_{j\sigma}^\dagger \hat{c}_{j\sigma} + \hat{c}_{j\sigma}^\dagger \hat{f}_{j\sigma}) + \varepsilon_f \sum_{j,\sigma} \hat{n}_{j\sigma}^f \\ & + U_f \sum_j \hat{n}_{j\uparrow}^f \hat{n}_{j\downarrow}^f, \end{aligned} \quad (1)$$

where the notation is standard and $W = 4t$ is taken as the energy unit. The spin and charge gaps of the one-dimensional PAM have been studied by several methods in the past decades. The exact diagonalization studies³ pointed out that both the charge and spin gaps are finite. This analysis was later confirmed and refined by the density-matrix renormalization-group calculations⁴⁻⁶. Both methods showed that the charge gap is always larger than the spin gap, and decreases much more slowly than the spin gap as U_f is increased and their ratio diverges in the large U_f limit. Later on,

this inequality was rigorously proven for the ordinary periodic Anderson model and it was shown that it remains valid for a d -dimensional simple cubic lattice as well.⁷ The charge and spin gaps are also directly measurable quantities using optical and neutron scattering measurements, respectively. It is worth noting that for numerous compounds the experimental ratio of the gaps is less than one, which is in qualitatively good agreement with the theoretical predictions for the one-dimensional PAM, and in some cases, like CeRu₄Sb₁₂ or CeFe₄Sb₁₂, even quantitative agreement can be achieved with the theoretical predictions.⁸ However, for CeRhAs the ratio of the spin⁹ and charge gaps¹⁰ was found to be greater than one, namely, $\Delta_s/\Delta_c \approx 1.5$, which cannot be understood at all in the frame of the ordinary periodic Anderson model.⁸ One of the major aims of the present paper is to provide a possible explanation to the problem.

Several extensions of the PAM have been considered lately, to model the effect of further electron-electron interactions. The role of conduction electron interaction in the Kondo lattice model and PAM has been thoroughly investigated.^{11,12} Recently, the correlations between conduction and f electrons have been shown to play an important role to understand the critical valence fluctuations.¹³ This interaction term leads to the extended PAM (EPAM):

$$\mathcal{H} = \mathcal{H}_{\text{PAM}} + U_{cf} \sum_{j,\sigma,\sigma'} \hat{n}_{j\sigma}^f \hat{n}_{j\sigma'}^c. \quad (2)$$

This model has been investigated by several modern techniques recently,¹⁴⁻¹⁸ and the valence transition has been explained successfully. However, less attention has been paid to the Kondo insulator case.^{18,19} It has been shown recently using dynamical mean-field theory (DMFT), which is exact for infinitely large dimensions that in the symmetric case for small hybridization ($V \ll W$)

the model displays antiferromagnetic order for small U_{cf} which, however, disappears for large U_{cf} and charge order develops. In the charge ordered phase doubly occupied c and f sites appear in an alternating fashion, since the c and f electrons tend to avoid each other. Since these results were obtained via DMFT, which neglects spatial fluctuations, one can naturally ask what happens in low-dimensional systems, where the fluctuations are more important.

Our purpose in this paper is therefore to examine the one-dimensional EPAM. Naturally, we do not address the possibility of the presence of long-range order that was found in infinite dimensions. We apply the density-matrix renormalization-group method²⁰ (DMRG), which is a powerful tool to find the ground state and the first few excited states. Further advantage of the DMRG method is that we can determine the von Neumann entropies^{21–24} of single and multisite subsystems, which turned out to be very good indicators of drastic changes in the wavefunction.^{25–28} They are known to exhibit anomalous behavior where the character of the ground state changes dramatically.

The setup of the paper is as follows. In Sec. II. our numerical results are presented for the spin and the charge gaps of the extended periodic Anderson model. In Sec. III. A we investigate the spin and density correlation functions. In Sec. III. B we perform a quantum information analysis and determine the entanglement map of the EPAM using the mutual information^{29–31} to get a physical picture for the ground state. Lastly, in Sec. IV. our conclusions are presented.

II. SPIN AND CHARGE GAPS

For convenience the EPAM has been implemented in the DMRG procedure as a generalized Hubbard model with a special topology. The site i with both c and f electrons is replaced by two DMRG sites, one for the conduction electrons, the other for the f electrons, and therefore instead of working with 16 states per site, only 4 states per DMRG sites have to be considered. These $|\alpha\rangle$ states are the empty, singly occupied with down and up spin, and the doubly occupied states, denoted by $|0\rangle$, $|\downarrow\rangle$, $|\uparrow\rangle$, $|\uparrow\downarrow\rangle$, respectively,

$$\begin{aligned} |1\rangle^{(c)} &= |0\rangle, & |1\rangle^{(f)} &= |0\rangle, \\ |2\rangle^{(c)} &= |\downarrow\rangle_i^{(c)} = \hat{c}_{i\downarrow}^\dagger |0\rangle, & |2\rangle^{(f)} &= |\downarrow\rangle_i^{(f)} = \hat{f}_{i\downarrow}^\dagger |0\rangle, \\ |3\rangle^{(c)} &= |\uparrow\rangle_i^{(c)} = \hat{c}_{i\uparrow}^\dagger |0\rangle, & |3\rangle^{(f)} &= |\uparrow\rangle_i^{(f)} = \hat{f}_{i\uparrow}^\dagger |0\rangle, \\ |4\rangle^{(c)} &= |\uparrow\downarrow\rangle_i^{(c)} = \hat{c}_{i\uparrow}^\dagger \hat{c}_{i\downarrow}^\dagger |0\rangle, & |4\rangle^{(f)} &= |\uparrow\downarrow\rangle_i^{(f)} = \hat{f}_{i\uparrow}^\dagger \hat{f}_{i\downarrow}^\dagger |0\rangle. \end{aligned} \quad (3)$$

The schematic structure is shown in Fig. 1. In what follows the chain length N is understood as the number of real EPAM sites. In our DMRG calculations, we apply the dynamic block-state selection algorithm^{32,33} and keep block states up to 2000, the typical truncation errors are $10^{-6} - 10^{-8}$. Open boundary condition is applied, and

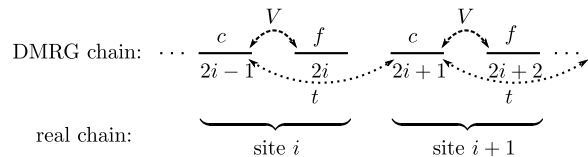


FIG. 1. Sketch of the DMRG implementation of the model Hamiltonian Eq. (2).

we considered chains up to a maximum length $N = 50$ and finite-size scaling is used to extrapolate the quantities to the thermodynamic limit.

In the following, we consider the half-filled symmetric EPAM for moderately large U_f . We address first the effect of U_{cf} on the spin and charge gaps of the EPAM. The spin gap is defined as

$$\Delta_s = E_0(S = 1, N_e) - E_0(S = 0, N_e), \quad (4)$$

where $E_0(S, N_e)$ denotes the ground-state energy in the given (S, N_e) subspace, where S and N_e are the total spin and particle number, respectively. The latter one is $N_e = 2N$ in the half-filled case. It is known that the ordinary PAM possesses an extra $SU(2)$ symmetry³, and the charge gap can be calculated from the expression:

$$\Delta_c = [E_0(S = 0, N_e + 2) + E_0(S = 0, N_e - 2) - 2E_0(S = 0, N_e)]/2. \quad (5)$$

This extra symmetry, however, is no longer present in the EPAM, and therefore we have to apply the general definition of the charge gap⁴:

$$\Delta_c = E_n(S = 0, N_e) - E_0(S = 0, N_e) \quad (6)$$

where $E_n(S = 0, N)$ is the energy of the lowest excited state $|n\rangle$, for which $S = 0$ and $\langle n | \sum_q \rho_q | 0 \rangle \neq 0$, where ρ_q is the q Fourier component of the charge density operator:

$$\rho_q = \sum_{i=0}^{N-1} e^{-iqr_i} \left[\hat{c}_{i\uparrow}^\dagger \hat{c}_{i\uparrow} + \hat{c}_{i\downarrow}^\dagger \hat{c}_{i\downarrow} + \hat{f}_{i\uparrow}^\dagger \hat{f}_{i\uparrow} + \hat{f}_{i\downarrow}^\dagger \hat{f}_{i\downarrow} \right]. \quad (7)$$

This definition of the charge gap is motivated by the fact that in optical measurements this gap is obtained by measuring the conductivity, which is related to the charge density. The spin and charge gaps as a function of U_{cf} are shown in Fig. 2. The charge gap is not calculated far below the crossing point, since the corresponding charge excitation lies much higher than the spin gap. As for the spin gap, it gets very small for small values of U_{cf}/W . As shown in Fig. 3 a linear extrapolation in $1/N$ to infinite chain length seems to give a finite spin gap for any U_{cf}/W . The number of data points used in the extrapolation depends on the scaling of the block entropy and the a priori set accuracy threshold value. As the gap gets smaller, it becomes increasingly difficult to determine it accurately for small values of U_{cf} using the DMRG algorithm. Nevertheless, we see a clear

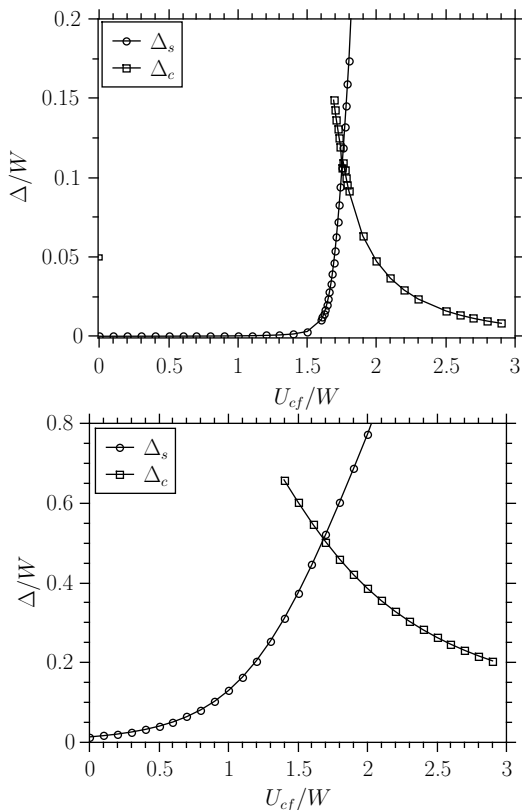


FIG. 2. The spin and charge gaps extrapolated to the thermodynamic limit as a function of U_{cf} for $V/W = 0.1$ (upper panel), $V/W = 0.3$ (lower panel) and $U_f/W = 3$. The lines are guides to the eye.

tendency as demonstrated in Fig. 4 that the spin gap increases monotonically with U_{cf}/W for all system sizes we considered. Since we know that the spin gap is finite for $U_{cf} = 0$, $\Delta_s \sim e^{-\pi t U_f / 4\alpha V^2}$, where α is a scaling constant,³ we conclude that the spin gap is always finite. In the one-dimensional model, in contrast to the DMFT results,¹⁸ there is no signature of quantum phase transition and the ground state is always a spin singlet.

Since Δ_s increases with U_{cf} , while Δ_c decreases, they cross at a value $U_{cf}^{cr} \approx U_f/2 + W/4$. It can be seen that this crossing point slightly shifts toward smaller U_{cf} values as V is increased. The sharp increase of the spin gap around and above the crossing point can be understood as follows. Here the c and f electrons try not to occupy the same site. Since the total number of f electrons is N in the symmetric model, and the same holds for the conduction electrons, the two kinds of electrons can best avoid each other by dominantly occupying every second site, the odd sites with two f electrons and the even sites with two conduction electrons, or vice versa. Since the doubly occupied sites are necessarily in a singlet state, a spin flip can be achieved by transferring an electron to another site and a local singlet has to be broken up for that. For U_{cf} larger than the value at the crossing point, there are a large number of singlet excited states

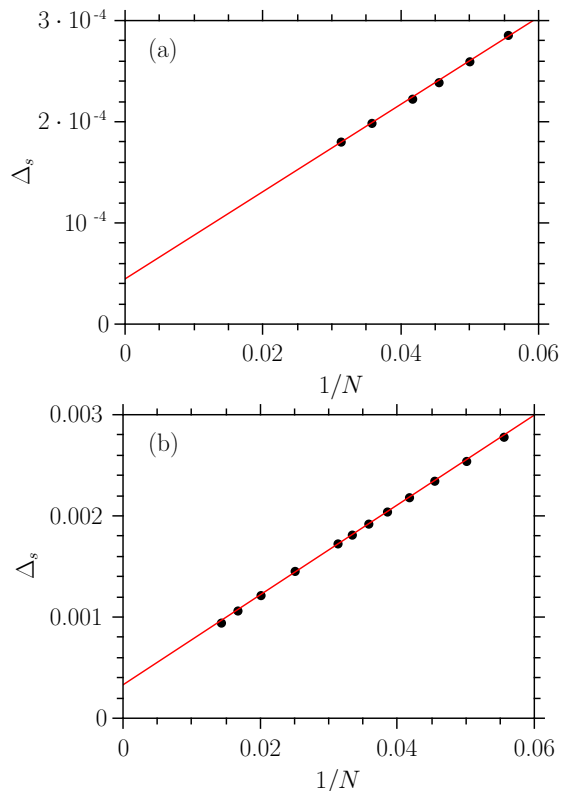


FIG. 3. Finite-size extrapolation of the spin gap for $U_{cf}/W = 1$ (panel (a)), $U_{cf}/W = 1.5$ (panel (b)). The solid lines denote the linear fits to the data.

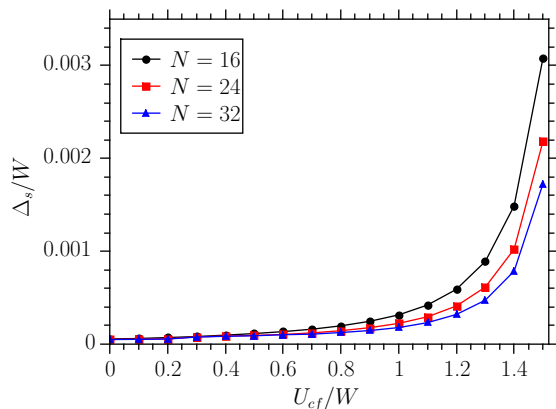


FIG. 4. (color online) The spin gap as a function of U_{cf} , for several chainlengths at $V/W = 0.1$, $U_f/W = 3$.

with lower energy. They determine the density-density correlations and therefore the gap to the lowest of them is considered as the charge gap, in agreement with Eq. (6). This gap decreases and tends to zero for $U_{cf} \rightarrow \infty$.

III. CORRELATION FUNCTIONS AND ENTANGLEMENT PATTERNS

A. Correlation functions

As a next step we investigate the correlation functions, which provide a further insight into the effects of interorbital interaction. The spin and density correlation functions are defined in the usual way:

$$S_{ij}^{(ab)} = \langle \hat{S}_i^{(a)} \hat{S}_j^{(b)} \rangle = \left\langle \frac{1}{2} (a_{i\uparrow}^\dagger a_{i\downarrow} b_{j\downarrow}^\dagger b_{j\uparrow} + a_{i\downarrow}^\dagger a_{i\uparrow} b_{j\uparrow}^\dagger b_{j\downarrow}) + \frac{1}{4} (n_{i\uparrow}^{(a)} - n_{i\downarrow}^{(a)}) (n_{j\uparrow}^{(b)} - n_{j\downarrow}^{(b)}) \right\rangle \quad (8)$$

$$N_{ij}^{(ab)} = \langle \hat{n}_i^{(a)} \hat{n}_j^{(b)} \rangle - \langle \hat{n}_i^{(a)} \rangle \langle \hat{n}_j^{(b)} \rangle, \quad (9)$$

where a and b stand for either f or c and $\hat{n}_i^{(a)} = \sum_\sigma \hat{n}_{i\sigma}^{(a)}$. The correlation functions oscillate with periodicity $2a$ (a is the lattice constant) as seen in Fig. 5 and their amplitude decays exponentially since the system is gapped for any value of U_{cf} . The behavior of the amplitude of

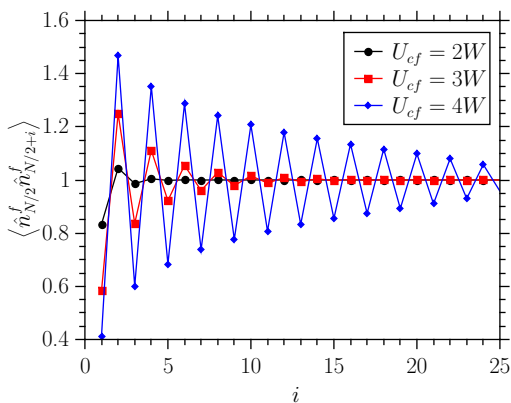


FIG. 5. (color online) The density correlation function for different values of U_{cf} and $N = 50$ chain length. The other parameters are fixed at $V/W = 0.1$ and $U_f/W = 3$. The lines are guides to the eye.

the correlation functions is shown in Fig. 6. The decrease or increase of the gap with U_{cf} is reflected in the variation of the decay length. A naive estimate of the correlation length from the linear fit to the data would give $\xi/a \approx 200$, for $U_{cf} = 0$. Although such a large decay length cannot be obtained reliably from calculations on chains with 50 sites, it can be taken as an order of magnitude estimate, corroborating our expectations. Namely, such large values of ξ can be explained with the known behavior of the ordinary PAM. As has been pointed out,⁵ the correlation length of the spin correlation function increases exponentially by increasing U_f .

As long as U_{cf} is below the crossing point the spin correlation function is dominant due to the tiny spin gap. The spin correlation length decreases while the density correlation length increases as U_{cf} is increased. Above

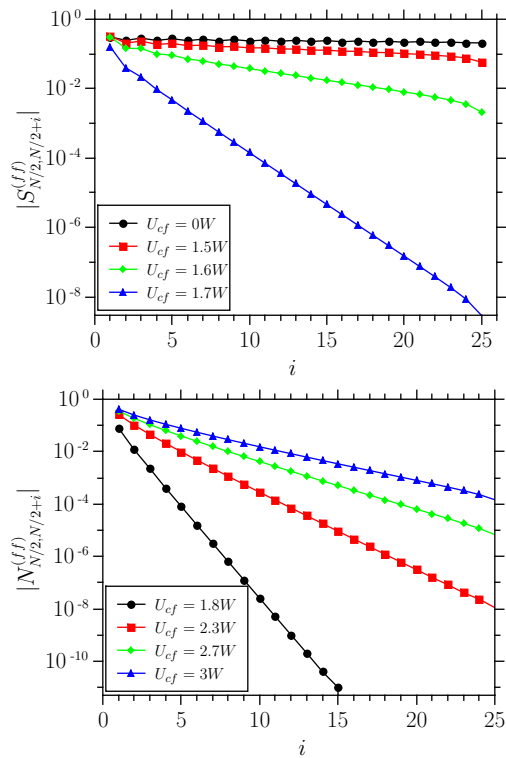


FIG. 6. (color online) The upper and lower panel show the spin and density correlation functions respectively for different values of U_{cf} and $N = 50$ chain length. The other parameters are fixed at $V/W = 0.1$ and $U_f/W = 3$. The lines are guides to the eye.

the crossing point, the density correlation function has the longer correlation length which corresponds to the peculiar behavior of the charge gap. Knowing that one cannot have true long-range order in one dimension, but slowly decaying correlations might indicate ordering in higher dimensions, we might guess that strong U_{cf} leads to charge ordering, as indeed it was found in the DMFT calculation.¹⁸

It is interesting to examine the spin correlation between f and conduction electrons on the same site. This is shown in Fig. 7. It is obvious from the figure that the local singlet correlation is enhanced significantly near U_{cf}^{cr} , which confirms the DMFT results.¹⁸ This behavior is not expected in the conventional PAM, since it can be mapped to the Kondo lattice model with weak Kondo coupling, and the appearance of a Kondo-singlet-like state is expected at strong Kondo couplings. Therefore the corresponding Kondo-coupling becomes much stronger at the crossing point.

B. Quantum information analysis

In this section we investigate the behavior of the von Neumann entropies of various subsystem configurations, which are very reliable tools for detecting drastic changes

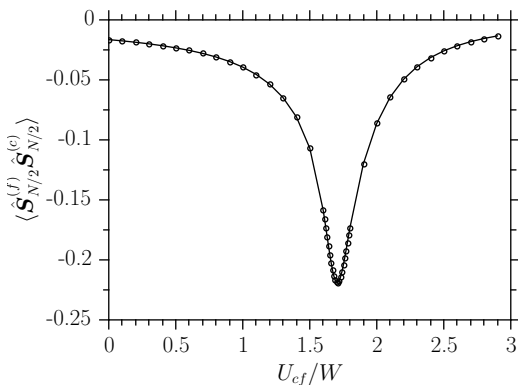


FIG. 7. The onsite spin correlation between conduction and f electrons (extrapolated to the thermodynamic limit) for $V = 0.1W$ as a function of U_{cf} and $U_f/W = 3$. The lines are guides to the eye.

of the ground state and analyzing its structure. We examined the one-site s_i and two-site s_{ij} entropies, which can be obtained from the appropriate reduced density matrices.^{21,26} The entropy of a single site can be obtained as

$$s_i = -\text{Tr}\rho_i \ln \rho_i, \quad (10)$$

where ρ_i is the reduced density matrix of site i , which is derived from the density matrix of the total system by tracing out the configurations of all other sites. We also define the c- and f-parts of the site entropies ($s_i^{(c)}$, $s_i^{(f)}$) in the following way:

$$s_i^{(c)} = -\text{Tr}\rho_i^{(c)} \ln \rho_i^{(c)}, \quad (11)$$

$$s_i^{(f)} = -\text{Tr}\rho_i^{(f)} \ln \rho_i^{(f)}, \quad (12)$$

where $\rho_i^{(c)}$ ($\rho_i^{(f)}$) is obtained by performing an additional trace over the remaining f (c) degrees of freedom. The two-site entropy is written as

$$s_{ij} = -\text{Tr}\rho_{ij} \ln \rho_{ij}, \quad (13)$$

where ρ_{ij} is the two-site reduced density matrix of sites i and j . We can also introduce the partial two-site entropies for c or f electrons on site i and c or f electrons on site j :

$$s_{ij}^{(ab)} = -\text{Tr}\rho_{ij}^{(ab)} \ln \rho_{ij}^{(ab)}, \quad a, b \in \{c, f\} \quad (14)$$

where $\rho_{ij}^{(ab)}$ is derived from ρ_{ij} by tracing out the states of the other electrons. The DMRG implementation described in the beginning of Sec. II. enables us to determine $s_i^{(a)}$ and $s_{ij}^{(ab)}$ separately. The mutual information which measures the entanglement between sites i and j can be obtained from:

$$I_{ij} = s_i + s_j - s_{ij}, \quad (15)$$

while the mutual information between a and b type electrons on sites i and j is defined as

$$I_{ij}^{(ab)} = s_i^{(a)} + s_j^{(b)} - s_{ij}^{(ab)}, \quad (16)$$

which measures the entanglement between a and b type electrons on sites i and j .

At first we consider the single site entropies, which are shown in Fig. 8. For small V the entropy of f electrons

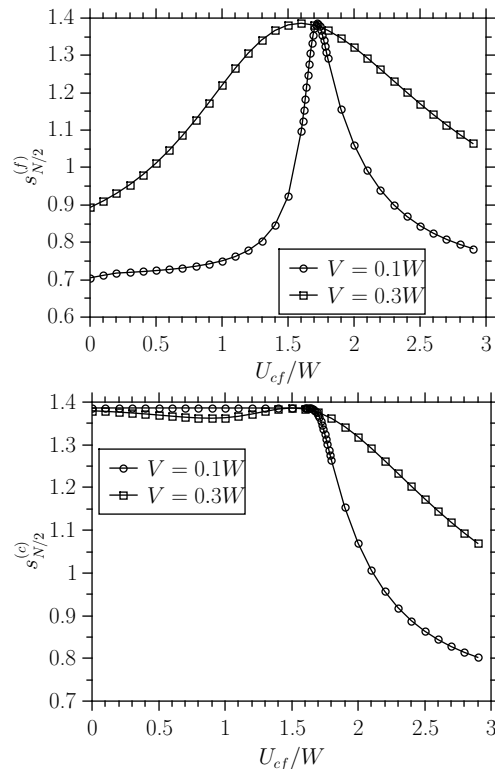


FIG. 8. The extrapolated f (upper panel) and c (lower panel) site entropies as a function of U_{cf} , for $U_f/W = 3$. The lines are guides to the eye.

starts from slightly above $\ln 2$. When $U_{cf} = 0$ the f electrons are strongly correlated and since the f-level occupancy must be exactly one (in the symmetric model), only one electron with up or down spin can occupy the f level. Due to the small c-f hybridization the entropy of f electrons is slightly higher than $\ln 2$, since a small number of doubly occupied levels can also be present. Switching on U_{cf} leads to the appearance of more and more doubly occupied f sites, so the entropy begins to increase. At a certain value of U_{cf} , which is the crossing point defined earlier, a peak is developed, where the entropy of f electrons takes its maximum value, $\ln 4$, then it begins to decrease and approaches $\ln 2$ again, since for large U_{cf} an f site is expected to be either doubly occupied or empty. For larger hybridization this sharp maximum is significantly broadened. Concerning the conduction electrons, their entropy is $\ln 4$ as long as $U_{cf} < U_{cf}^{\text{cr}}$, since they are free particles. Above the crossover value, the probability of finding zero or two c electrons on the same site

increases from $1/4$ to $1/2$, so correlation is developed between c electrons. It is readily observed that there should be a remarkable change in the ground state, where the entropy of f electrons has a maximum.

We also examined the one-site entropy of the EPAM, and it is shown in Fig. 9. For weak hybridization it

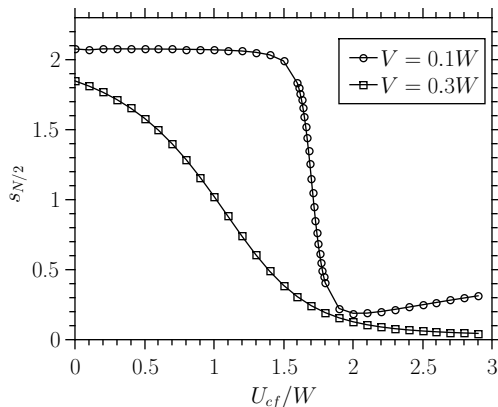


FIG. 9. The extrapolated one-site entropies, for two different values of hybridization and $U_f/W = 3$. The lines are guides to the eye.

drops rather drastically around U_{cf} corresponding to the crossover point and then starts to increase slowly, while for stronger hybridization the decrease of the site entropy is less drastic. But in both cases s_i is much smaller above U_{cf}^{cr} than below this value. A nearly vanishing s_i is indication that the wave function is dominated by terms localized to this site.

To better reveal the reason of these anomalies we calculated the mutual information between c and f type electrons on sites i and j for several values of U_{cf} . The mutual information for $U_{cf} = 0$ is shown in Fig. 10 for weak hybridization. It is easy to observe that moderately strong but short-ranged entanglement is developed between c electrons and much weaker between c and f electrons due to the small hybridization. On the other hand long-ranged but weaker entanglement is formed between the f electrons. This is the consequence of the strong RKKY-interaction, which results in the antiferromagnetic correlations between the f electrons; the f electrons form a collective singlet.

The mutual information diagram has an entirely different structure for $U_{cf} = 1.75W \approx U_{cf}^{cr}$, which is shown in Fig. 11. One can see that there is a strong entanglement between c and f electrons on the same site. The entanglement bonds between the sites are much weaker. According to the entanglement map, the ground-state wave function becomes approximately a product state. We will determine the structure of the onsite state later. Lastly, we consider the case when $U_{cf} = 4W > U_{cf}^{cr}$. The mutual information is shown in Fig. 12. Here we observe that the strong onsite entanglement remains, however, moderately strong bonds appear between neighbouring c and f sites. It is worth noting, that the magnitude of

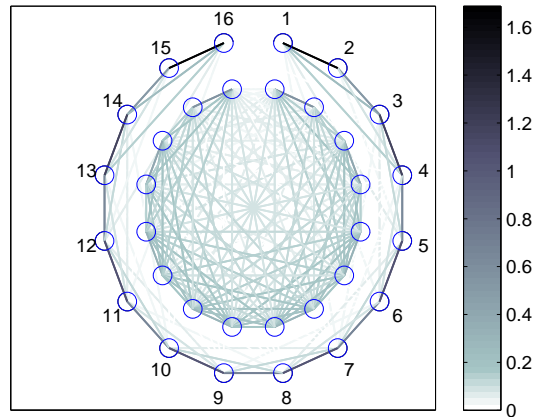


FIG. 10. (color online) Schematic view of all components of the mutual information ($I_{ij}^{(cc)}$, $I_{ij}^{(cf)}$, $I_{ij}^{(ff)}$) for $U_{cf} = 0$, $V/W = 0.1$, $U_f/W = 3$ and $N = 16$. The inner and outer circles denote f and c sites, respectively. The numbers denote the real EPAM sites.

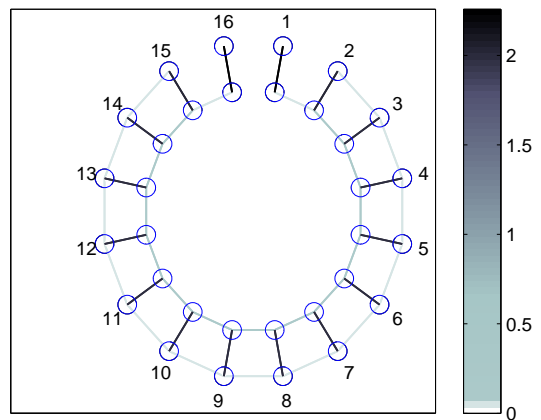


FIG. 11. (color online) Schematic view of all components of the mutual information ($I_{ij}^{(cc)}$, $I_{ij}^{(cf)}$, $I_{ij}^{(ff)}$) for $U_{cf} = 1.75W$, $V/W = 0.1$, $U_f/W = 3$ and $N = 16$. The inner and outer circles denote f and c sites respectively. The numbers denote the real EPAM sites.

the entanglement of the onsite bonds is $\mathcal{O}(1)$, while it is $\mathcal{O}(10^{-3})$ for the next largest entanglement bond when $U_{cf} = 3W$, $V = 0.3W$ and $U_f = 3W$, that is, every other bond is smaller by two orders of magnitude.

The above statements can be quantified if we introduce the following quantity:

$$I_{\text{dist}}^{(m)} = \frac{1}{N} \sum_{ab} \sum_{ij} I_{ij}^{(ab)} (i-j)^m. \quad (17)$$

$I_{\text{dist}}^{(m)}$ is the m th momentum of the distribution $I_{ij}^{(ab)}$, which measures the localization of the entanglement. Its

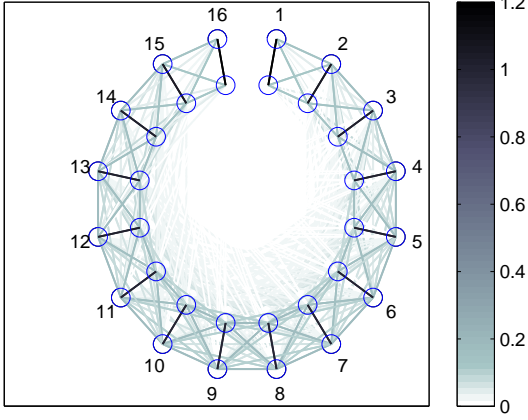


FIG. 12. (color online) Schematic view of all components of the mutual information ($I_{ij}^{(cc)}$, $I_{ij}^{(cf)}$, $I_{ij}^{(ff)}$) for $U_{cf} = 4W$, $V/W = 0.1$, $U_f/W = 3$ and $N = 16$. The inner and outer circles denote f and c sites respectively. The numbers denote the real EPAM sites.

values for different values of U_{cf} and m are shown in Table I. It is easily seen that the entanglement is most

U_{cf}/W	$I_{\text{dist}}^{(2)}$	$I_{\text{dist}}^{(4)}$
0	50.7	4169.9
1.75	0.24	0.38
4	19.1	959.0

TABLE I. The different momenta of $I_{ij}^{(ab)}$ for several values of U_{cf} and $V = 0.1W$.

localized when $U_{cf} = 1.75W$. In the other two cases the entanglement is much more delocalized.

These conclusions have been obtained for finite systems, therefore we have to investigate the finite-size effects. For $U_{cf} = 0$ the entanglement bonds show strong dependence on the chain length, while for $U_{cf} = 1.75W$ and $4W$ the above results are very close the bulk limit for $N = 16$ already. The size dependence of the bonds for $U_{cf} = 0$ is shown in Fig. 13.

One can naturally ask what the relevant physical process is in creating the strong onsite bonds around the crossing point and for stronger U_{cf} . To answer this question we examined the eigenvalues (ω_α , $\alpha = 1, \dots, 16$) of the two-site density matrix $\rho_{ij}^{(ab)}$. For $U_{cf} = 0$ we found that several eigenvalues of $\rho_{N/2N/2}^{(cf)}$ are of the same order of magnitude and the eigenvectors contain all basis states $|\alpha_c, \alpha_f\rangle$, except for $|0, 0\rangle$ and $|\uparrow\downarrow, \uparrow\downarrow\rangle$. However, for $U_{cf} = 1.75W$ one of the eigenvalues of $\rho_{N/2N/2}^{(cf)}$ becomes almost two orders of magnitude larger than the

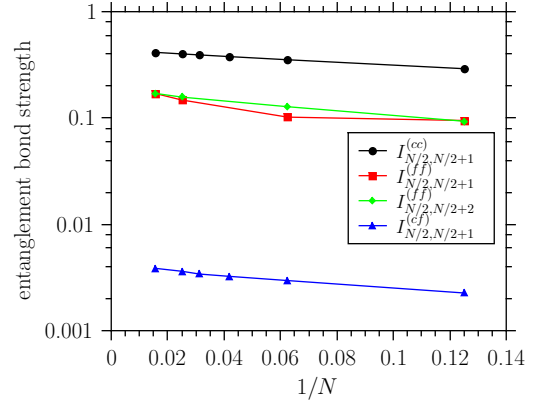


FIG. 13. (color online) The finite-size scaling of various entanglement bond for $U_{cf} = 0$, $V = 0.1W$ and $U_f/W = 3$. The lines are guides to the eye.

others. The corresponding eigenfunction reads:

$$\begin{aligned} \phi_{N/2N/2}^{(cf)} = & -0.5798(|\uparrow\downarrow, 0\rangle + |0, \uparrow\downarrow\rangle) \\ & -0.4048(|\uparrow, \downarrow\rangle - |\downarrow, \uparrow\rangle). \end{aligned} \quad (18)$$

It is seen that the configuration in which the site is occupied with two f electrons in a singlet state or two conduction electrons in a singlet state has roughly the same weight as the state in which a conduction and an f electron form a singlet. The latter configuration was observed in the spin correlation function in Fig. 7 and corresponds to the enhanced spin Kondo-effect. The former one describes the fluctuations between the doubly occupied and empty c-f configurations. Further increase of U_{cf} results in the suppression of the singlet part in Eq. (18). For example for $U_{cf} = 4W$, the eigenfunction corresponding to the most significant eigenvalue is:

$$\begin{aligned} \phi_{N/2N/2}^{(cf)} = & 0.7049(|\uparrow\downarrow, 0\rangle + |0, \uparrow\downarrow\rangle) \\ & -0.0561(|\uparrow, \downarrow\rangle - |\downarrow, \uparrow\rangle). \end{aligned} \quad (19)$$

Parallel with the suppression of the c-f singlets, two f or two conduction electrons occupy more and more this site. This is the reason why strong onsite entanglement bonds appear in Fig. 12.

In addition, as has been shown in Ref. [34] one can also analyze the sources of entanglement encoded in $I_{ij}^{(ab)}$ by studying the behavior of the matrix elements of $\rho_{ij}^{(ab)}$. They can be expressed in terms of the generalized correlation functions of $\mathcal{T}_i^{\alpha'\alpha(a)}$ and $\mathcal{T}_j^{\beta'\beta(b)}$, where $\mathcal{T}_i^{\alpha'\alpha(a)}$ is the transition matrix that transfers state $|\alpha\rangle^{(a)}$ ($\alpha = 1 \dots 4$ and $a \in \{c, f\}$) defined in Eq. (3) into state $|\alpha'\rangle^{(a)}$ on the same site i , while all other matrix elements vanish. For example

$$\mathcal{T}_i^{(2,3)(c)}|3\rangle^{(c)} = \mathcal{T}_i^{(2,3)(c)}\hat{c}_{i\uparrow}^\dagger|0\rangle = \hat{c}_{i\downarrow}^\dagger|0\rangle = |2\rangle^{(c)} \quad (20)$$

and

$$\mathcal{T}_i^{(3,4)(f)}|4\rangle^{(f)} = \mathcal{T}_i^{(3,4)(f)}\hat{f}_{i\uparrow}^\dagger\hat{f}_{i\downarrow}^\dagger|0\rangle = \hat{f}_{i\uparrow}^\dagger|0\rangle = |3\rangle^{(f)}. \quad (21)$$

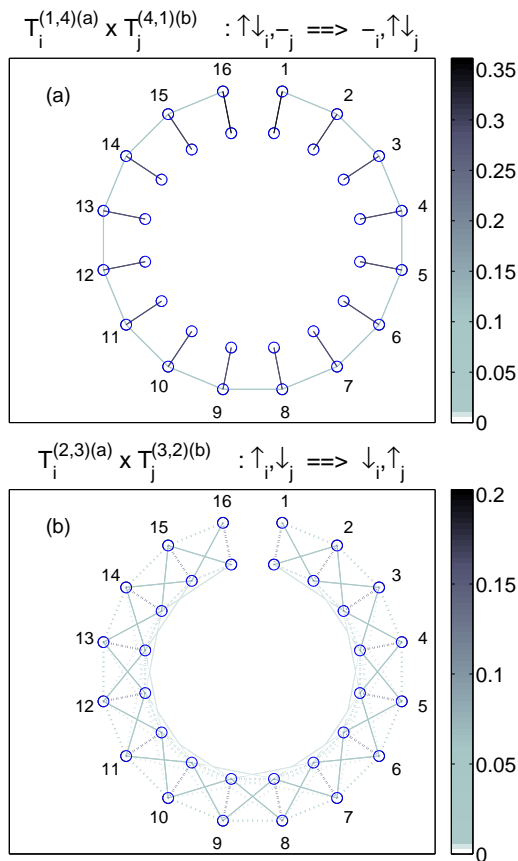


FIG. 14. (color online) Pictorial representation of two generalized correlation functions: $\langle \mathcal{T}_i^{(1,4)(a)} \mathcal{T}_j^{(4,1)(b)} \rangle_C$ (panel (a)) and $\langle \mathcal{T}_i^{(2,3)(a)} \mathcal{T}_j^{(3,2)(b)} \rangle_C$ (panel (b)). The parameters are $U_{cf} = 1.75W$, $V/W = 0.1$, $U_f/W = 3$ and $N = 16$. The inner and outer circles denote f and c sites, respectively. The positive and negative values of the correlations are shown by solid and dotted lines, respectively. The numbers denote the real EPAM sites.

We studied the connected part of the generalized correlation functions, $\langle \mathcal{T}_i^{\alpha' \alpha(a)} \mathcal{T}_j^{\beta' \beta(b)} \rangle_C = \langle \mathcal{T}_i^{\alpha' \alpha(a)} \mathcal{T}_j^{\beta' \beta(b)} \rangle - \langle \mathcal{T}_i^{\alpha' \alpha(a)} \rangle \langle \mathcal{T}_j^{\beta' \beta(b)} \rangle$, where the disconnected part, given by the product of the expectation values of local transition operators, is subtracted. We demonstrate here, that these can be used to identify the relevant physical processes that lead to the generation of entanglement. Namely, we show the correlation functions of two different transition operators giving the largest contribution to $\rho_{ij}^{(ab)}$. One of them describes the hopping of a down- and up-spin electron pair, the other one is a spin-flip. The matrix elements of these operators are shown in Figs. 14 and 15. It is clearly seen that the correlations in spin-flip processes are significantly reduced as U_{cf} is increased. At the same time the fluctuations of the up- and down-spin electron pairs is enhanced. These results support our previous findings derived from the analysis of the eigensystem of the two-site density matrix $\rho_{ij}^{(ab)}$.

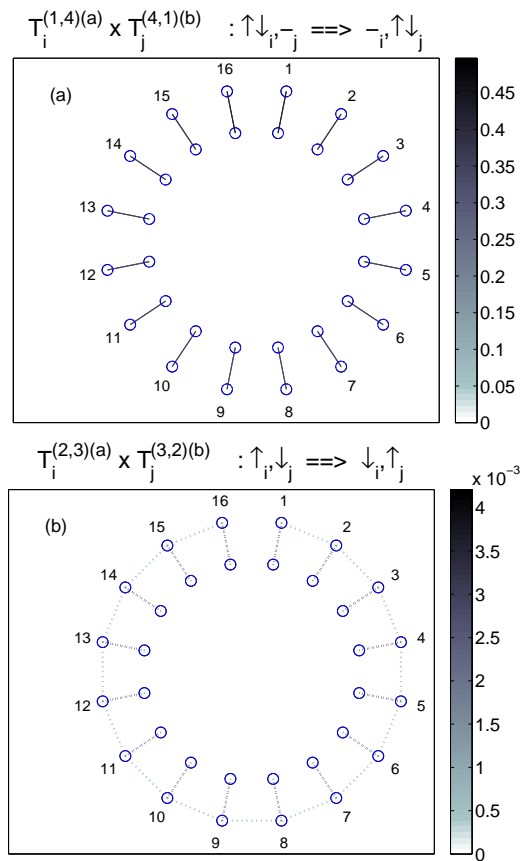


FIG. 15. (color online) The same as in Fig. 14, but for $U_{cf} = 4W$.

The decay of the mutual information is governed by the smallest gap in the model. The fastest decay is found for $U_{cf} \approx U_{cf}^{cr}$, where both the spin and charge gaps are large. For other U_{cf} values we observed a slower decay, which is in agreement with the behavior of the gaps. We observed that the mutual information decays as the square of the most slowly decaying correlation functions at long distances in agreement with the results of Ref. [34].

IV. CONCLUSIONS

In this paper we investigated an extended periodic Anderson model, where the interaction between conduction and f electrons, U_{cf} , has been included. Our aim was to examine the properties of the model in one dimension by applying the density matrix renormalization group algorithm. As a first step, we investigated the spin and charge excitations of the model. It turned out that the model is always gapped. The spin gap, Δ_s , is much smaller than the charge gap, Δ_c , for small U_{cf} . Since Δ_s increases with U_{cf} while Δ_c decreases, they cross at some value of U_{cf} and the charge gap gets smaller. This result may give a possible explanation for the anomalous behavior

of the gaps observed in CeRhAs, where $\Delta_s/\Delta_c > 1$ was measured. The crossing point shifts only slightly as the hybridization becomes stronger.

As a next step, the spin and density correlation functions have been determined. Below the crossing point the spin correlation function is dominant due to strong antiferromagnetic coupling mediated by the RKKY interaction. As U_{cf} is increased the spin correlation length decreases, while the density correlation length increases and becomes dominant above the crossing point. In higher dimensional systems, especially in DMFT calculations, the dominance of the spin or charge excitations leads to two distinct ordered phases. In the DMFT results, an antiferromagnetic–charge order transition was found, moreover the position of this critical point strongly depends on the hybridization. In one dimension we have found, however, no sign of phase transition. In our model the correlation functions always decay exponentially, but we can distinguish two regimes depending on which decay length is larger.

Finally, we performed a quantum information analysis to reveal the structural changes in the ground state wave function. The one-site entropy of c and f electrons varies rapidly around the point where the spin and charge gaps

are equal. The entropy of f electrons has a maximum there, while the entropy of c electrons starts to decrease rapidly. We calculated the mutual information for several c-f interaction strengths, which measures the entanglement between different sites. It turned out that for small hybridization the wave function is approximately a product state consisting of strongly localized states at the sites. For larger U_{cf} the strong onsite entanglement remains, which originates from the tendency of charge ordering, the preference of having two f electrons on even sites and two c electrons on odd sites or vice versa.

ACKNOWLEDGMENTS

This work was supported in part by the Hungarian Research Fund (OTKA) through Grant Nos. K 100908 and NN110360. The research of I. H. was supported by the European Union and the State of Hungary, co-financed by the European Social Fund in the framework of TÁMOP-4.2.4.A/ 2-11/1-2012-0001 'National Excellence Program'. I. H. acknowledges fruitful discussions with A. Kiss and K. Itai.

-
- ¹ P. S. Riseborough, Adv. in Phys. **49**, 257 (2000).
² For reviews on this topic see, for example, P. Fulde, J. Keller, and G. Zwicknagl, in *Solid State Physics: Advances in Research and Applications*, edited by H. Ehrenreich and D. Turnbull (Academic Press, San Diego, 1988), Vol. 41, pp. 1-150; P. Fazekas, *Lecture Notes on Electron Correlation and Magnetism* (World Scientific, Singapore 1999); A. C. Hewson, *The Kondo Problem to Heavy Fermions* (Cambridge University Press, Cambridge, 1993); H. Tsunetsugu, M. Sigrist, and K. Ueda, Rev. Mod. Phys. **69**, 809 (1997).
³ T. Nishino and K. Ueda, Phys. Rev. B **47**, 12451 (1993).
⁴ M. Guerrero and C. C. Yu, Phys. Rev. B **51**, 10301 (1995).
⁵ P. R. Bertussi, M. B. Silva Neto, T. G. Rappoport, A. L. Malvezzi, R. R. dos Santos, Phys. Rev. B **84**, 075156 (2011).
⁶ N. Shibata and K. Ueda, J. Phys.: Condens. Matter **11**, R1 (1999).
⁷ G.-S. Tian, Phys. Rev. B **58**, 7612 (1998).
⁸ D. T. Adroja, K. A. McEwen, J.-G. Park, A. D. Hillier, N. Takeda, P. S. Riseborough, T. Takabatake, J. Opt. and Adv. Mat., **10**, 1719 (2008).
⁹ D. T. Adroja, J.-G. Park, K. A. McEwen, K. Shigetoh, T. Sasakawa, T. Takabatake, J.-Y. So, Physica B, **378-380**, 788 (2006).
¹⁰ H. Okamura, M. Matsunami, T. Nanba, T. Suemitsu, T. Yoshino, T. Takabatake, Y. Isikawa, H. Harima, Physica B, **312-313** 218 (2002).
¹¹ N. Shibata, T. Nishino, K. Ueda, C. Ishii, Phys. Rev. B **53**, 8828(R) (1996).
¹² T. Schork and P. Fulde, Phys. Rev. B **50**, 1345 (1994).
¹³ K. Miyake, J. Phys.: Condens. Matter **19**, 125201 (2007).
¹⁴ S. Watanabe, M. Imada, and K. Miyake, J. Phys. Soc. Japan **75**, 043710 (2006), S. Watanabe, M. Imada, and K. Miyake, J. Magn. and Magn. Mat. **310**, 841 (2007).
¹⁵ Y. Saiga, T. Sugibayashi, and D. S. Hirashima, J. Phys. Soc. Japan **77**, 114710 (2008).
¹⁶ V. N. Phan, A. Mai, and K. W. Becker, Phys. Rev. B **82**, 045101 (2010).
¹⁷ K. Kubo, J. Phys. Soc. Japan **80**, 114711 (2011).
¹⁸ T. Yoshida and N. Kawakami, Phys. Rev. B **85**, 235148 (2012).
¹⁹ I. Hagymási, K. Itai, and J. Sólyom, Phys. Rev. B **87**, 125146 (2013).
²⁰ S. R. White, Phys. Rev. Lett. **69**, 2863 (1992); Phys. Rev. B **48**, 10345 (1993).
²¹ Ö. Legeza and J. Sólyom, Phys. Rev. B **68**, 195116 (2003).
²² G. Vidal, J. I. Latorre, E. Rico, and A. Kitaev, Phys. Rev. Lett. **90**, 227902 (2003).
²³ P. Calabrese and J. Cardy, J. Stat. Mech.: Theor. Exp. P06002 (2004).
²⁴ L. Amico, R. Fazio, A. Osterloh, V. Vedral, Rev. Mod. Phys. **80**, 517 (2008).
²⁵ M.-F. Yang, Phys. Rev. A. **71**, 030302(R) (2005).
²⁶ Ö. Legeza and J. Sólyom, Phys. Rev. Lett. **96**, 116401 (2006).
²⁷ N. Laflorencie, E. S. Sørensen, M.-S. Chang and I. Affleck, Phys. Rev. Lett. **96**, 100603 (2006).
²⁸ J. Vidal, G. Palacios, and R. Mosseri, Phys. Rev. A **69**, 022107 (2004), J. Vidal, R. Mosseri, and J. Dukelsky, Phys. Rev. A **69**, 054101 (2004).
²⁹ J. Rissler, R. M. Noack, and S. R. White, Chem. Phys. **323**, 519 (2006).
³⁰ G. Barcza, Ö. Legeza, K. H. Marti, M. Reiher, Phys. Rev. A **83**, 012508 (2011).
³¹ K. Boguslawski, P. Tecmer, G. Barcza, Ö. Legeza, and M. Reiher, J. Chem. Theory Comp. **9** 2959-2973 (2013).

³² Ö. Legeza, J. Röder, and B. A. Hess, Phys.Rev. B **67**, 125114 (2003).

³³ Ö. Legeza and J. Sólyom, Phys. Rev. B **70**, 205118 (2004).

³⁴ G. Barcza, R. M. Noack, J. Sólyom, Ö. Legeza, arXiv:1406.6643.